Supporting information

Cationic Polarity Facilitation with Tailored Aminopyridine Ligands for Bulkier Defect-Free and Air-Stable Perovskite Solar Cells

Wei-Hsiang Chen,[1] Lei Ning,[2] Liang Chen,[2] Pei-Cheng Jiang,[3,4] Cheng-Hsun-Tony Chang,[5] Pingfan Du,[2] Lixin Song,[*2] Jie Xiong[*2]

Materials and Preparation

Materials

The glass/FTO substrates, Lead (II) iodide (PbI_2, 99.99%), and [6,6]-phenyl-C61-butyric acid methyl ester ($PC_{61}BM$, 99%) were purchased from Advanced Electronic Technology Co., Ltd. Dimethylformamide (DMF, 99.8%), ethanol (EtOH, 99.7%), ethyl acetate (EA, 99.5%), acetone (99%), dimethyl sulfoxide (DMSO, 99.7%), isopropanol (IPA, 99.7%), and acetonitrile (ACN, 99.5%) were bought from Aladdin. Formamidinium iodide (FAI, 99.5%), methylammonium chloride (MACl, 99.5%), methylammonium bromide (MABr, 99.5%), cesium iodide (CsI, 99.99%), lead bromide ($PbBr_2$, 99.99%), poly[bis-(4-phenyl)-(2, 4, 6 trimethylphenyl)-amine] (PTAA, M_w : 6000-15000), 2,2′,7,7′-Tetrakis(*N*,*N*-di-*p*-methoxyphenylamine)-9,9′-spirobifluorene (spiro-OMeTAD, 99.5%), 4-tert-butylpyridine (TBP, 96%), lithium bis(trifluoromethanesulfonyl)imide (Li-TFSI, 99.95%), and octylamine hydrobromide (OABr, 99.5%) were purchased from Xi′an Yuri Solar Co., Ltd. SnO_2 colloidal

solution (15% in water) was bought from Alfa Aesar. 2,6-Bis(aminomethyl)pyridine (2,6-BAMPy, 98%) was purchased from Bidepharm. 4-Isopropyl-4′-methyldiphenyliodonium tetrakis(pentafluorophenyl)borate (TPFB, 98%) was purchased from Tokyo Chemical Industry.

Preparation of perovskite precursor

$Cs_{0.05}FA_{0.90}MA_{0.05}Pb(I_{0.95}Br_{0.05})_3$ triple-cation perovskite was utilized in this work. The perovskite precursor (1.4 M) was composed of CsI, FAI, MABr, PbI_2 and $PbBr_2$ in the mixed solvent of DMF/DMSO (v/v, 4/1). Additional MACl (35%) and PbI_2 (10%) were incorporated for better perovskite crystallization. This perovskite precursor should be stirred for 6 h at room temperature and carefully filtered through a 0.22 μm PTFE filter before usage.

Preparation of spiro-OMeTAD solution

To prepare spiro-OMeTAD mixed solution, 72.3 mg spiro-OMeTAD was disolved into 1 mL anhydrous CB solution with the addition of 17.5 μL Li-TFSI solution (520 mg/mL in anhydrous ACN solution) and 28.8 μL TBP, followed by 30 min of stirring before use.

Device fabrication

The FTO-etched glass substrates were sequentially cleaned by ultrasonic bath with detergent, DI water, acetone, and ethanol for 20 min, respectively, and then dried in the hot plate. Afterward, the substrates were treated by ultraviolet (UV) ozone for 45 min to further clear up the organic residue on the top. SnO_2 colloidal solution (SnO_2/DI water/H_2O_2, v/v/v, 1/4/1) was first spin-coated onto FTO glass substrate with a

rotational speed of 4000 rpm for 30 s, and then annealed at 150 ℃ for 30 min in ambient air to obtain the SnO_2 electron transport layer (ETL). To exclude other impacts from buried interface mismatch and possible interaction between 2,6-DMPy$[(FA)_2]^{2+}$ (within bottom perovskite) with SnO_2 at the buried interface, appropriate concentrations of 2,6-BAMPy molecule in IPA was spin-coated on top of SnO_2 ETL with a speed of 5000 rpm for 30 s, followed by 100 °C annealing treatment for 2 min.[1] After that, the well-prepared perovskite precursor with or without 2,6-BAMPy incorporation (detail mentioned above) was spin-coated on SnO_2/FTO substrate with a speed of 1000 rpm for 10 s and increased to 5000 rpm for 30 s. During the second step of spin-coating, 245 μL EA (function as antisolvent) was dynamically pipetted onto the perovskite for 20 s before the end of spin-coating operation. For the 2,6-BAMPy-treated samples, 2,6-BAMPy was added into perovskite precursor with optimal concentration. After one-step antisolvent washing, the as-prepared perovskite films were heated at 100 °C for 30 min. Upon cooling down to room temperature, perovskite films were passivated by dynamically spin-coating OABr solution (2 mg/mL in IPA) and annealing at 100 °C for 5 min. Subsequently, 60 μL of spiro-OMeTAD solution was spin-coated onto the top of perovskite films with the rotational speed of 3000 rpm for 30 s to form the hole transport layer (HTL). Finally, a 100 nm Ag electrode with an active area of 0.06 cm^2 was deposited by thermal evaporation. All devices were fabricated in the open-air environment (30-40% relative humidity) at room temperature (20-25 °C).

Characterization

Measurement of PSC efficiency

The photocurrent density-voltage (*J-V*) characteristics of the devices were measured by a Keithley 2400-SCS source meter with an AM 1.5 solar simulator coupled with 450 W xenon lamp (Newport-2612A). *J-V* curves were measured in forward and reverse scan by the scan speed of 0.01 v/s in ambient air environment (30-40% relative humidity). For incident-photon-to-current conversion efficiency measurement, a Newport Instruments system (Newport-74125) equipped with a lock-in amplifier and a 300 W xenon lamp was conducted.

Stability test

The operational stability test for unencapsulated devices was performed under a consecutive 1-sun illumination (a light-emitting diode (LED) lamp without UV filter) in open-air. In stability tests, the spiro-OMeTAD was taken place by PTAA layer. The PTAA (20 mg/mL) solution was prepaerd with the addition of 10 wt% TPFB and then spin-coated with the rotational speed of 3000 rpm for 30 s. The damp-heat stability tests for encapsulated PSCs was conducted at 85 °C and 85% RH in the constant temperature and humidity test chamber (HS-408L) for 2400 h. The PSCs were encapsulated in an N_2 atmosphere by UV adhesive (LT-U001, Lumtec) and a glass on top.

Density functional theory calculations

The density functional theory (DFT) calculations were carried out with the VASP code.[2] The Perdew-Burke-Ernzerhof (PBE) functional within generalized gradient approximation (GGA) was used to process the exchange-correlation, while the projectoraugmented-wave pseudopotential (PAW) was applied with a kinetic energy cut-off of 500 eV, which was utilized to describe the expansion of the electronic

eigenfunctions.[3-4] The Brillouin-zone integration was sampled by a Γ-centered 1 × 1 × 1 Monkhorst-Pack k-point. All atomic positions were fully relaxed until energy and force reached a tolerance of 1×10^{-5} eV and 0.05 eV/Å, respectively.

The adsorption energy (E_{ads}) of a complex formed between two molecules, A and B, can be calculated using the following equation:

$$E_{ads} = E_{complex} - (E_A - E_B)$$

Where: $E_{complex}$ is the total energy of the molecular complex of A and B. E_A and E_B are the total energies of isolated molecules A and B, respectively.

The charge density of the optimized structures was analyzed using the Bader charge analysis method based on the electron density obtained from VASP calculations, to quantify the charge transfer between different atoms and adsorption species. And The Gibbs free energy was calculated as the difference in the Gibbs free energy of the system before and after the incorporation of the small molecule into the PbI lattice.

The formation energy was calculated as:

$$E_{form} = E_{compound} - xE_{bulk}$$

Where E_{form} is the total energy of the optimized structure, E_{bulk} represents the energy of the bulk phase. A negative E_{form} indicates that the compound is thermodynamically stable with respect to the bulk reference.

^{1}H nuclear magnetic resonance (^{1}H NMR) and Electrospray ionization mass spectroscopy (ESI-MS)

High-resolution liquid NMR spectrometer was measured by Bruker AVANCE (500 MHz), and all samples in this context were dissolved into DMSO-d6 solution for

measurements. For ESI-MS analysis, all samples were prepared in the mixed solvent of DMSO/IPA and analyzed with a Thermo Scientific Q-Exactive mass spectrometer. The spectra were eqipped with a resolution of 140000 at m/z 200 and an automatic gain control target of 1 million.

X-ray photoelectron spectra (XPS)

X-ray photoelectron spectroscopy (XPS, K-Alpha, USA) was conducted with a micro-focus monochromatic Al Kα X-ray source. The instrument resolution was 0.45 eV.

X-ray diffraction (XRD) and Scanning electron microscopy (SEM)

X-ray diffraction (XRD, Bruker D8 Advance) was measured with Cu Kα radiation with an angle range of 5-50° and scan rate of 3°/min. SEM images were performed by scanning electron microscope (Zeiss SUPRA 55) equipped with an electron beam with accelerated voltage at 3 kV, enabling operation at a variety of currents.

Electrochemical impedance spectroscopy (EIS) measurements

The EIS was conducted by potentiostat (Im6ex/Zahner) to investigate charge transfer and recombination with an alternative signal amplitude of 10 mV and a frequency range of 0.01-100 kHz.

Steady-state photoluminescence (PL) and time-resolved PL (TRPL) decay measurements

The steady-state PL spectrum was performed by Fluo Time 300 fluorophotometer Lifetime Spectrometer with 520 nm of excitation wavelength. TRPL decay was conducted by picosecond diode laser with 800 nm of excitation wavelength. The PL

decay curves can be well-fitted to biexponential decay function $I(t) = I_0 + A_1 exp^{(-t-t_0/\tau_1)} + A_2 exp^{(-t-t_0/\tau_2)}$. Generally, the fast decay constant τ_1 stands for free carrier quenching at the interface, while the slow decay constant τ_2 contributes to radiative recombination of the carrier. The average decay lifetime were obtained by following equation $\tau_{avg} = (\sum_i A_i \tau_i^2) \Big/ (\sum_i A_i \tau_i)$.

Other characterization

The trap filled limit voltages (V_{TFL}) were estimated through linear fitting of I-V responses. The trap density can be obtained via the following equation: $N_{defect} = 2\varepsilon_0 \varepsilon_r V_{TFL}/eL^2$, where ε_r presents the relative dielectric constant (~28.8), e contributes to electron charge, and L stands as thickness of the perovskite layer (~500 nm).

The light-intensity-dependent open-circuit voltage was measured for investigating carrier recombination within the PSC devices. The experimental data were well-fitted with the equation: $n = q/kT \times dV_{OC}/d(ln\varphi)$, where k stands for the Boltzmann constant, T presents the temperature, and q is the elementary charge.

Dark *J-V* measurements of the electron-only transport devices were collected for the observation of defect density and electron mobility of the perovskite films. The absorption spectra of perovskite films were measured by ultraviolet and visible spectrophotometry (UV-vis, P4, China). Mott-Schottky measurements (1000 Hz) were carried out on Chenhua electrochemical workstation (CHI 760E) under dark conditions.

Supplementary Note S1. Addition reaction between formamidinium (FA) unit and aminomethyl molecules

Based on the previous studies, methylamine moiety in aminomethyl derivatives can react with FA unit from perovskite through addition reaction.[5-7] It should be notable that due to the conjugating nature in symmetric FA^+ cation, the addition reaction is prone to producing two types of isomeric cationic products with specific resonance in $N_{FA}{}^+$ polarity.[6-7] The scheme in Figure S1a shows the addition reaction of FA^+ with methylamine. Figure S1b-c show the generalized addition reaction between FA^+ cation and a primary methylamine moiety with side group R or pyridine group RPy.

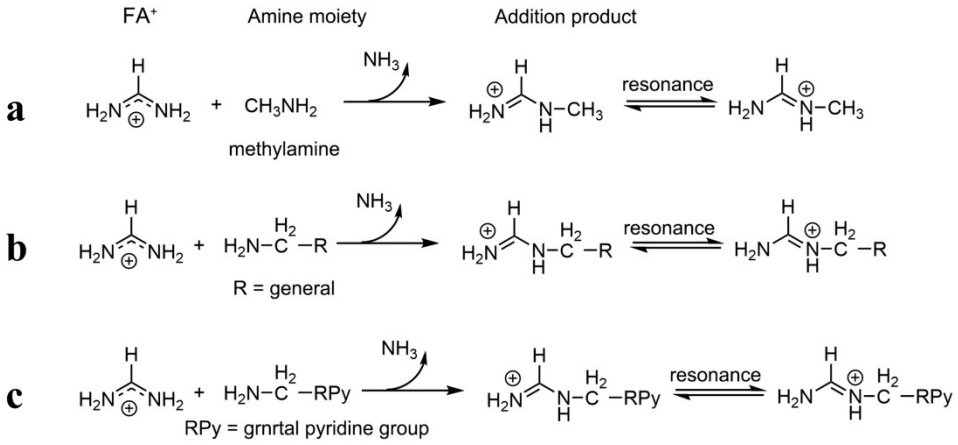

Figure S1. Addition reaction scheme. a) The addition reaction between conjugated FA^+ with methylamine, forming two types of isomeric MFA^+ and releasing ammonia (NH_3).[6] b) The generalized reaction. c) The generalized reaction with pyridine group.

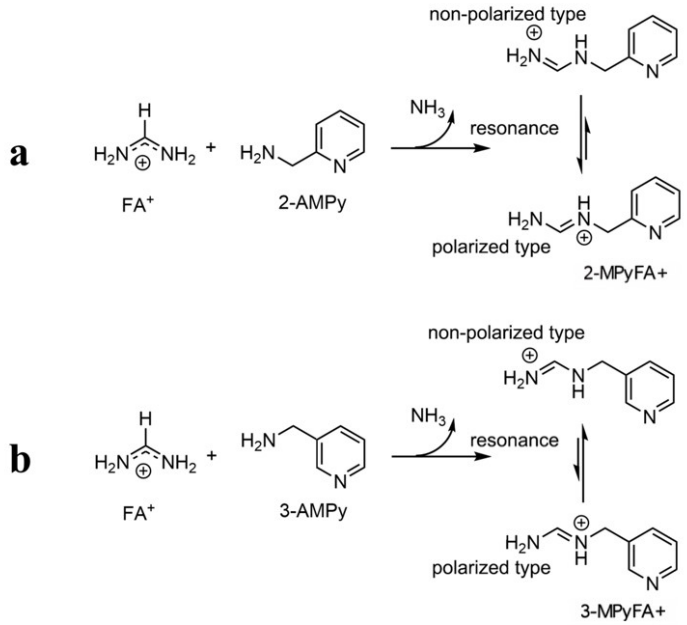

Figure S2. Addition reaction scheme. a) The addition reaction between conjugated FA^+ with 2-AMPy, forming two types of isomeric 2-$MPyFA^+$ dominated by polarized type. b) The addition reaction between conjugated FA^+ with 3-AMPy, forming two types of isomeric 3-$MPyFA^+$ dominated by non-polarized type.

Supplementary Note S2. Supplementary theoretical simulation of electron gain/loss status for other molecules similar to 2,6-BAMPy

In addition to the investigation of 2-AMPy and 2,6-BAMPy in this text, herein we also check the electron gain/loss of C_m for other similar aminopyridines, 2,6-bis(aminoethyl)pyridine (2,6-BAEPy) and 2,6-bis(aminopropyl)pyridine (2,6-BAPPy), both with a pair of alkylamine units attached at ortho positions of pyridine functional group as demonstrated in Figure S3. It can be seen that all the electron losses of C_m increases (0.287 and 0.318 in 2,6-BAEPy, 0.301 and 0.325 in 2,6-BAPPy) as compared with 2,6-BAMPy (0.052 and 0.094 in Figure 1b), indicating that 2,6-BAMPy is the most rational character triggering stable-one-type formation of amidinium cation with

enhanced N_{FA}^{+} polarity through addition reaction.

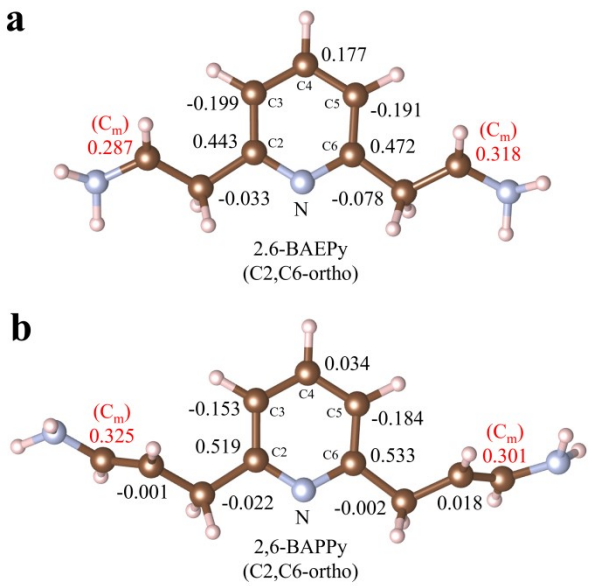

Figure S3. Electron gain/loss and molecular structure of a) 2,6-BAEPy, and b) 2,6-BAPPy molecules.

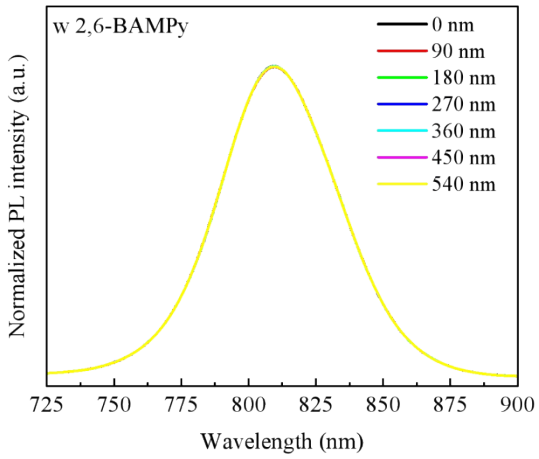

Figure S4. PL depth profile of confocal fluorescence microscope of perovskite film treated with 2,6-BAMPy.

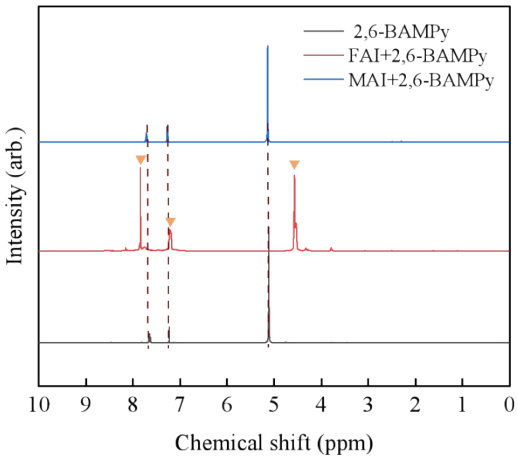

Figure S5. ^{1}H NMR spectra of 2,6-BAMPy, 2,6-BAMPy + MAI, and 2,6-BAMPy + FAI in DMSO-d6.

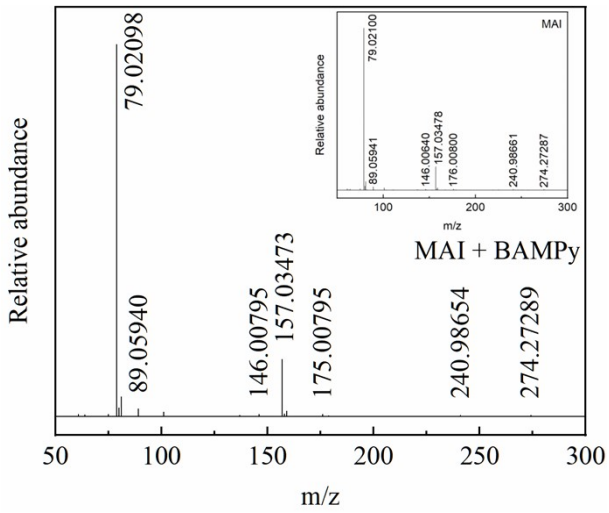

Figure S6. ESI-MS of 2,6-BAMPy (0.02 M) + MAI (0.1 M) sample with the inset image of pure MAI sample.

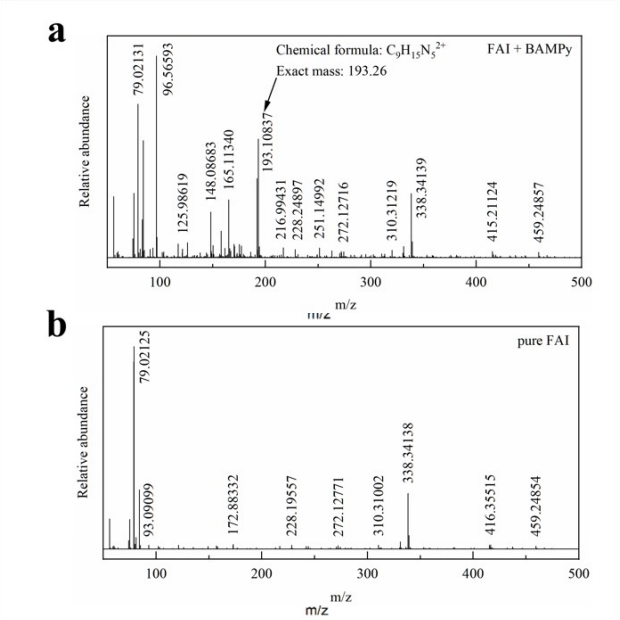

Figure S7. ESI-MS of a) 2,6-BAMPy (0.02 M) + FAI (0.1 M), and b) pure FAI sample.

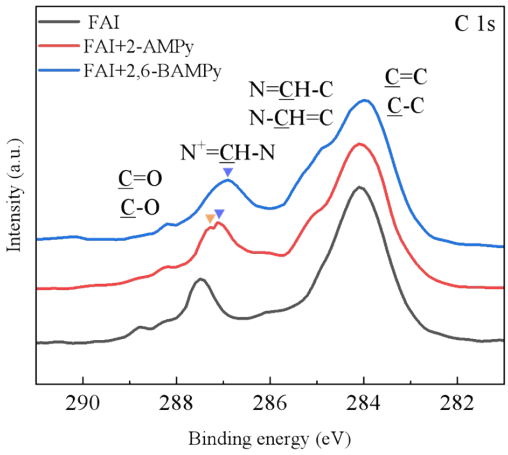

Figure S8. XPS C 1s core-level spectra for 2-AMPy + FAI, 2,6-BAMPy + FAI and pristine FAI films.

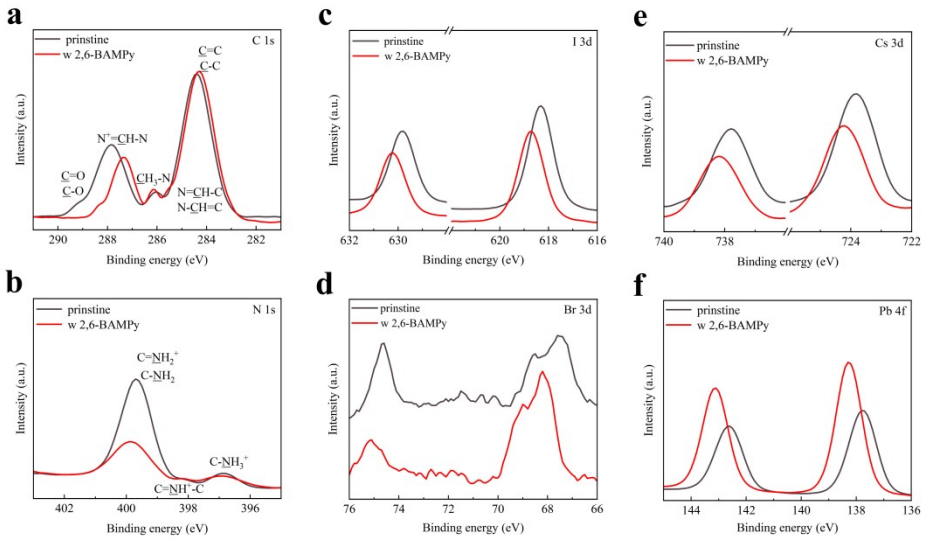

Figure S9. XPS core-level peaks of pristine and 2,6-BAMPy treated perovskite samples for a) C 1s, b) N 1s, c) I 3d, d) Br 3d, e) Cs 3d, and f) Pb 4f.

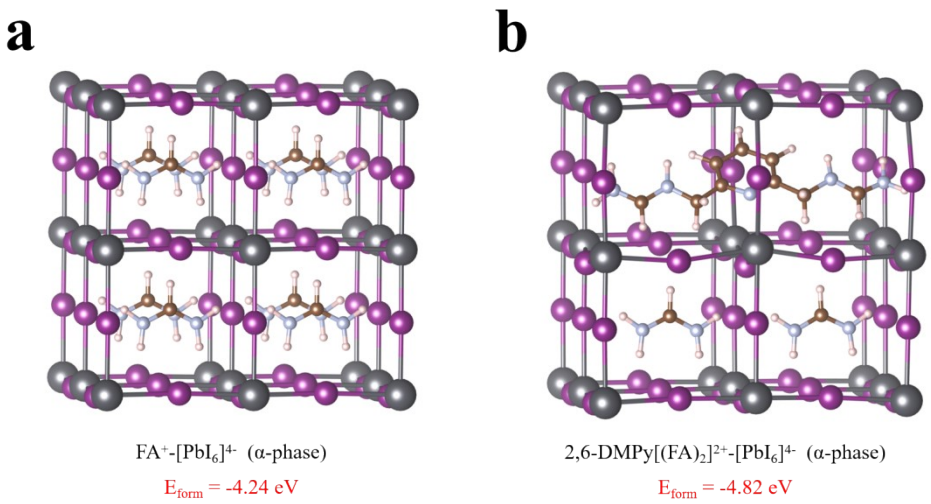

Figure S10. Calculated formation energy of ideal α-phase perovskite with a) typical $FAPbI_3$, and b) 2,6-BAMPy-processed $FAPbI_3$. In the models, deep purple (small), gray, white, indigo, violet represent C, N, H, Pb, I atoms, respectively.

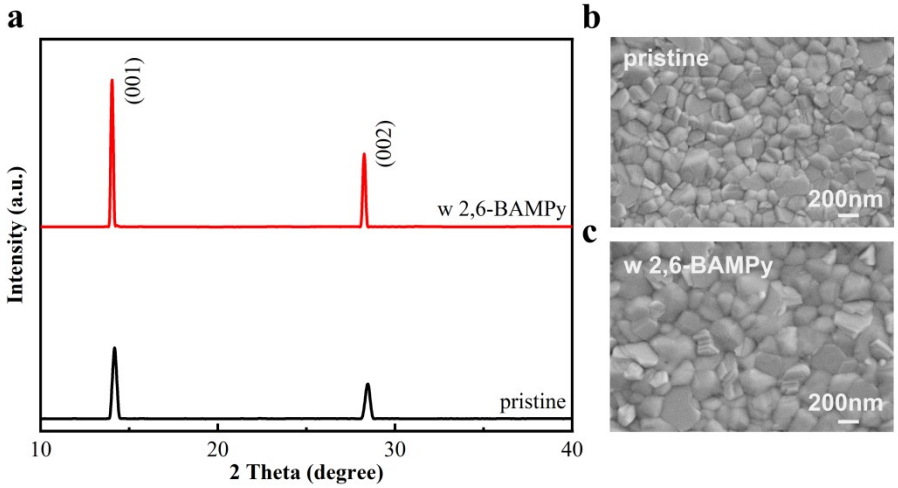

Figure S11. a) XRD spectra of perovskite films with or without 2,6-BAMPy treatment. Top-view SEM images of b) pristine, and c) 2,6-BAMPy-processed perovskite films.

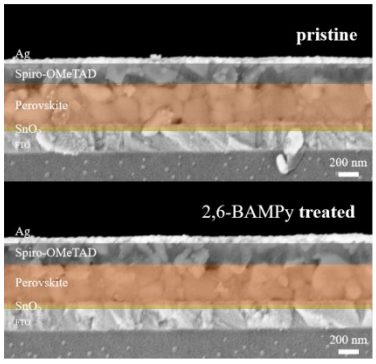

Figure S12. Cross-section SEM images of pristine, and 2,6-BAMPy-processed perovskite films.

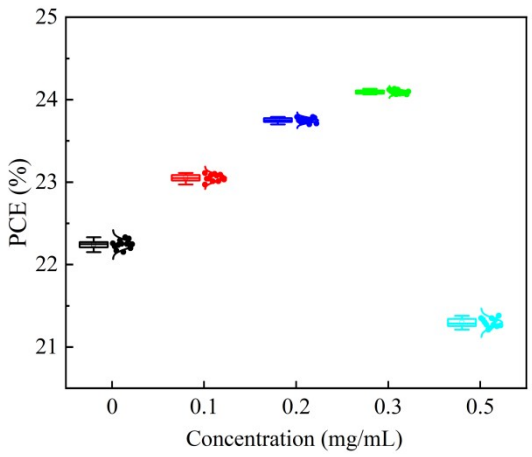

Figure S13. The statistic photovoltaic performances of PSC devices incorporated by

different concentration of 2,6-BAMPy.

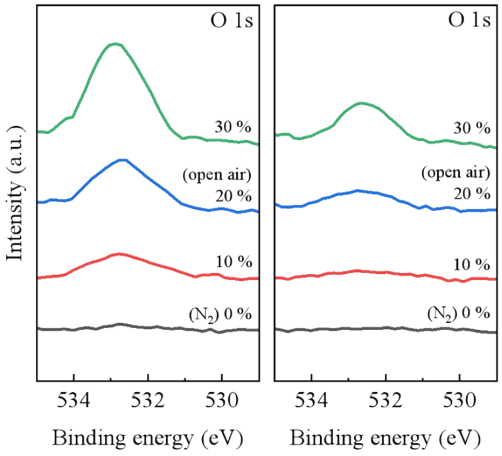

Figure S14. XPS O 1s core-level peaks of pristine and 2,6-BAMPy treated perovskite films fabricated under various levels of oxygen atmosphere. It can be seen that the smaller O 1s peaks with very slight signal increment through the increasing oxygen level can be observed for 2,6-BAMPy treated sample, indicative of the effective suppression in oxygen adsorption during the film fabrication.

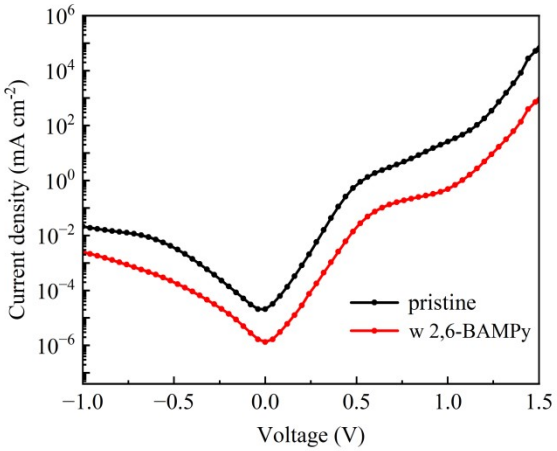

Figure S15. Dark *I-V* curves of PSCs with or without 2,6-BAMPy treatment.

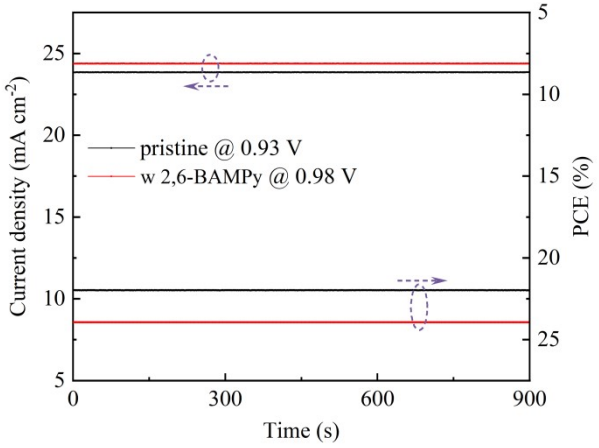

Figure S16. The stabilized power output of PSC devices with or without 2,6-BAMPy treatment.

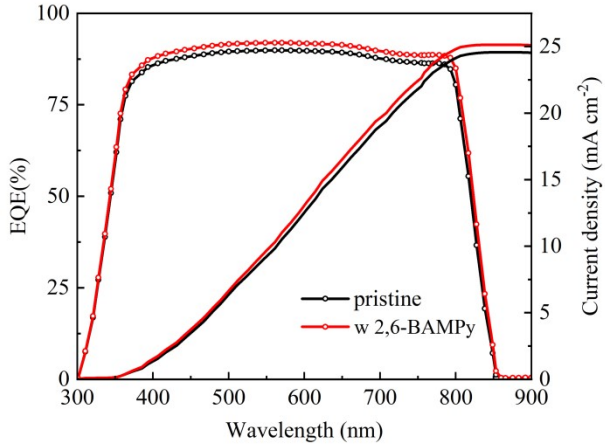

Figure S17. EQE spectra and integrated J_{sc} values of PSC devices with or without 2,6-BAMPy treatment.

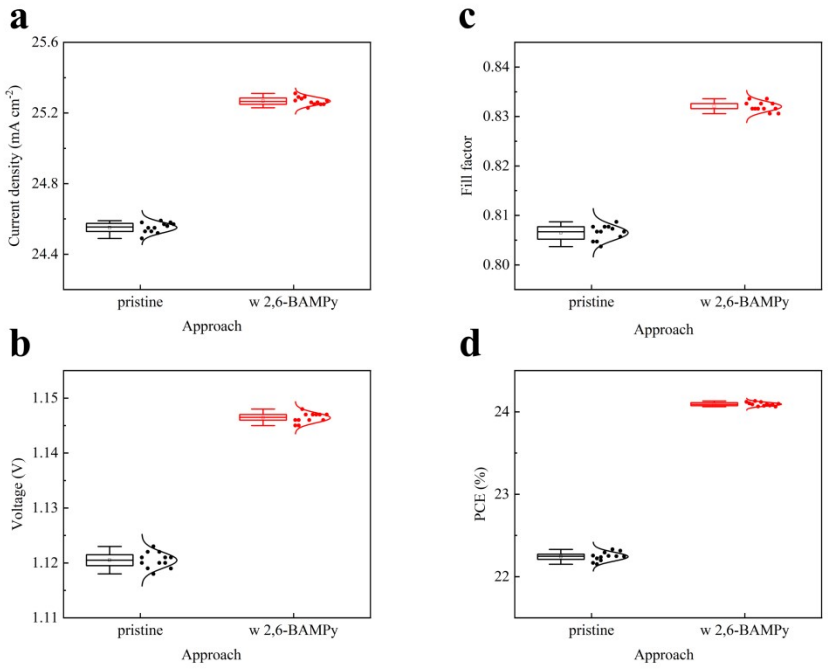

Figure S18. Statistical distribution of J_{sc}, V_{oc}, FF, and PCE values of PSCs with or without 2,6-BAMPy treatment.

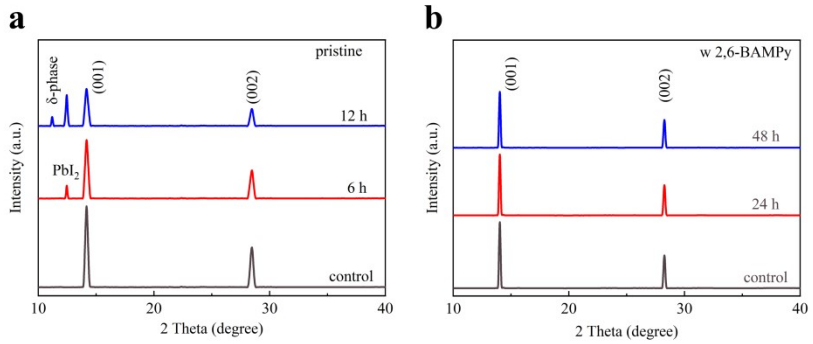

Figure S19. XRD spectra of a) pristine, and b) 2,6-BAMPy treated_perovskite films under different aging time in 120 ℃.

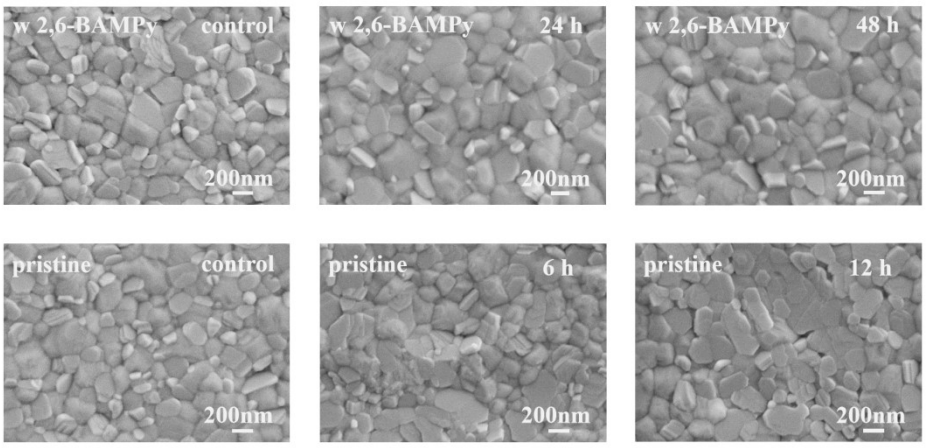

Figure S20. Top-view SEM images of a-c) pristine, and d-f) 2,6-BAMPy treated_perovskite films under different aging time in 120 ℃.

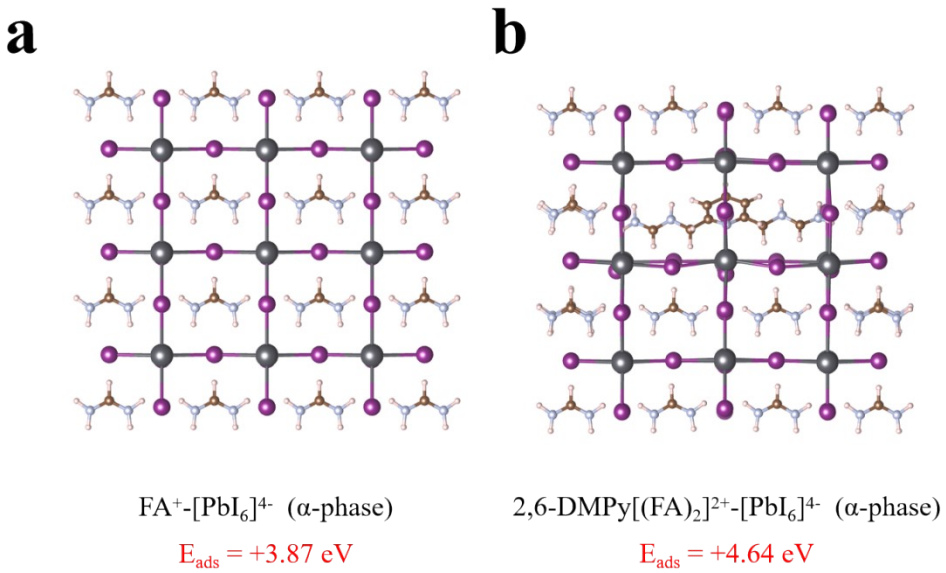

Figure S21. Calculated adsorption energy of ideal α-phase perovskite between a) pristine FA^+ and $[PbI_6]^{4-}$, and b) 2,6-DMPy$[(FA)_2]^{2+}$ and $[PbI_6]^{4-}$ framework. In the models, deep purple (small), gray, white, indigo, violet represent C, N, H, Pb, I atoms, respectively.

Reference

[1] L. Ning, L. X. Song, Z. Z. Yao, W. H. Chen, P. F. Du, P. C. Jiang, J. Xiong, *Adv. Energy Mater.* **2024**, *14*, 202401320.

[2] Furthmuller Kresse, *Phys. Rev. B* **1996**, *54*, 11169-11186.

[3] S. Grimme, J. Antony, S. Ehrlich, H. Krieg, *J. Chem. Phys.* **2010**, *132*, 3382344.

[4] S. Grimme, S. Ehrlich, L. Goerigk, *J. Comput. Chem.* **2011**, *32*, 1456-1465.

[5] Q. Jiang, J. H. Tong, Y. M. Xian, R. A. Kerner, S. P. Dunfield, C. X. Xiao, R. A. Scheidt, D. Kuciauskas, X. M. Wang, M. P. Hautzinger, et al. *Nature* **2022**, *611*, 278-283.

[6] V. Valenzano, A. Cesari, F. Balzano, A. Milella, F. Fracassi, A. Listorti, G. Gigli, A. Rizzo, G. Uccello-Barretta, S. Colella, *Cell Rep. Phys. Sci.* **2021**, *2*, 100432.

[7] X. Wang, Y. P. Fan, L. Wang, C. Chen, Z. P. Li, R. R. Liu, H. G. Meng, Z. P. Shao, X. F. Du, H. R. Zhang, et al. *Chem* **2020**, *6*, 1369-1378.